Design and testing of a latent heat storage for solar cooling applications

Andrea Frazzica[1], Valeria Palomba[1,2] and Vincenza Brancato[1]

[1]   CNR - Istituto di Tecnologie Avanzate per l'Energia "Nicola Giordano", Via Salita S. Lucia sopra Contesse 5, 98126 Messina, Italy.

[2]   Department of Engineering, University of Messina, C.da di Dio 98166 Messina

Abstract

The present paper reports the design, realization and testing of a lab-scale latent heat storage, specifically realized for solar cooling applications. The latent heat storage is based on a fin-and-tubes heat exchanger configuration employing a commercial paraffin as PCM. The paper mainly focuses on the experimental characterization, carried out by means of a test rig, available at the laboratory of the CNR ITAE, able to simulate working boundaries of a solar cooling plant. The experimental outcomes confirmed the increased heat storage density obtained by such a new component, compared to standard sensible heat storage. Nevertheless, still some limitations in the achievable heat transfer rate is highlighted, due to improper realization of the component.

Keywords: *heat storage, solar cooling, PCM*

1.   Introduction

During last years, an innovative technology, known as solar cooling, has gained more and more interest (Henning, 2007). Such a technology exploits the fact that cooling demand of buildings is in phase with the highest availability of solar irradiation during the year. Accordingly, it is possible to couple solar thermal collectors to thermally driven chillers for air conditioning applications (Henning et al., 2013). Usually, a closed cycle solar cooling plant is based on three main components, namely, the solar collectors field, the high temperature thermal energy storage and the thermally driven chiller (Henning et al., 2013). In the past, a lot of efforts have been paid to the identification of the optimal plant layout, in terms of surface of solar collectors, high temperature thermal energy storage size, backup system and thermally driven heat pump nominal power (Iranmanesh and Mehrabian, 2014; Hang et al., 2013). For solar cooling systems employing non-concentrating solar collector technologies (i.e. flat plane and evacuated tubes solar collectors), the high temperature heat storage relies on the sensible heat storage technique, mostly employing water as heat storage medium. Nevertheless, it is quite known that there are other opportunities to efficiently store heat. Among them, latent heat storage, based on the employment of phase change materials (PCMs) could be an interesting alternative (Mehling and Cabeza, 2008). Indeed, since they store and release heat in a narrow temperature range, they allow to feed the thermally driven chillers with an almost-constant temperature for long time, which can be beneficial for the performance of the chiller itself, increasing, at the same time, the heat storage density. Since in a solar cooling plant, the temperature difference between inlet and outlet on the heat storage side is limited to the temperature difference across the regenerator of the thermally driven chiller, which, from experimental outcomes, is usually around 10°C (Monnè et al., 2011), the employment of PCMs as heat storage medium seems quite reasonable.

Accordingly, in the present paper, the design, realization and testing of a lab-scale compact latent heat storage based on a fin-and-tube heat exchanger and a commercial paraffin is presented. Particularly, thanks

to a properly designed test rig, it was possible to verify the achievable performance under working conditions typical of a heat storage for solar cooling applications, both during charging and discharging phase.

2. Thermal storage system

2.1. Employed PCM

In the present paper, the studied PCM is the organic Plus-Ice A82 manufactured by PCM Products[®], whose nominal melting temperature, 82°C, perfectly suits the typical working range of solar cooling plants driven by non-concentrating solar thermal collectors. It consists in blend of linear and branched hydrocarbons. Its calorimetric features have been evaluated by means of a DSC-1 Mettler – Toledo. Ten milligrams of the material were tested cycling five times between 30°C and 110°C, with rate of 5°C/min, in static air and in a closed stainless steel pan sealed by means of a Viton[®] O-ring. The results reveal that the Plus-Ice A82 present good stability, with replicable latent heat and limited supercooling phenomenon. The measured melting enthalpy was 140 J/g, peak temperature during melting process was 85.7°C and peak temperature during solidification process was 80.8°C, thus showing slight supercooling. In order to take into account both sensible and latent heat, the integral heat curve between 40°C and 100°C was drawn, as reported in Figure 1. It is a useful tool to evaluate achievable heat storage density under different working boundary conditions. In the same figure, the mathematical fitting for the integral heat curve is represented, through which the theoretical energy for charge/discharge has been calculated.

$$y = -9E\text{-}08x^6 + 3E\text{-}05x^5 - 0.0047x^4 + 0.3419x^3 - 13.563x^2 + 277.82x - 2303.5$$
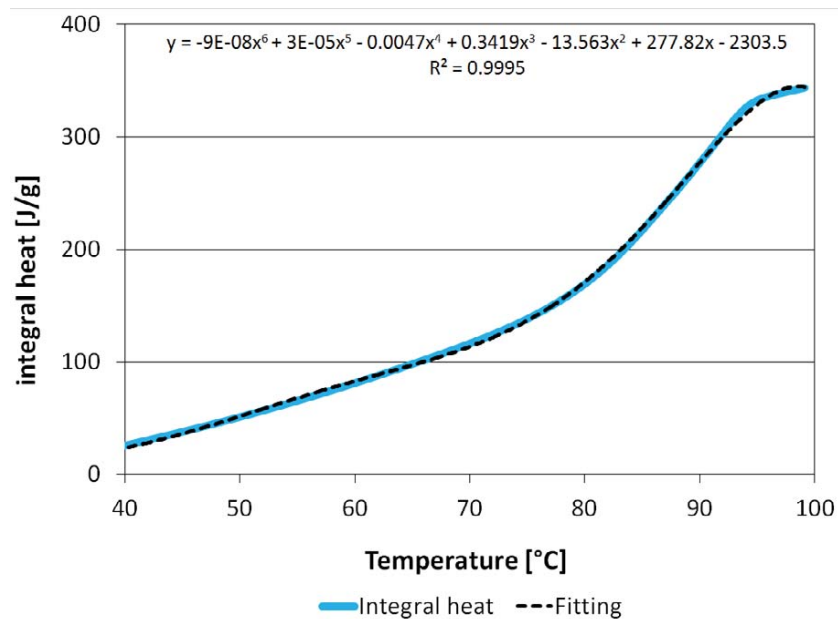$$R^2 = 0.9995$$

Figure 1: Integral curve of PCM PlusIce A82 and the numerical fitting.

2.2. Designed and realized prototype

In order to overcome the well-known limitations of low thermal conductivity of PCMs, in the present work, a fin-and-tube heat storage configuration has been designed through the aid of a detailed mathematical model.

In Figure 2, a 3D rendering of the storage and two picture of the realised system are presented, before and after the thermal insulation. The insulation has been realized with a 3 cm thick polymeric foam and by applying a layer of reflective aluminum foil.

Figure 2: the fin-and-tube heat exchanger for the latent storage, 3D rendering and pictures of the system before and after thermal insulation.

The main features of the storage are summarized in Table 1. It consists of 48 fins and 4 parallel hydraulic circuits, each one made up of 8 pipes, connected to the external sources via a manifold. Fin distance chosen is 5 mm, which allows to partially compensate for the low thermal conductivity of the chosen material. All the components are realized in AISI 416L.

Table 1: Main features of the fin-and-tube heat storage.

Material	AISI 416
Technology	Fin-and-tube heat exchanger with welded fins
Number of pipes	32
Diameter pipes	½ "
Ranks	4
Number fins	48
Fin dimensions	400 x 650 x 2 mm
Fin space	5 mm
Overall dimensions	400 x 650 x 350 mm
Overall weight	240 kg

8 thermocouples have been inserted inside the storage, their position chosen to highlight possible transversal and longitudinal temperature gradients, by distributing them along two different ranks and at different distances from the sides of the exchanger. The arrangement of the temperature sensors inside the storage is reported in Figure 3.
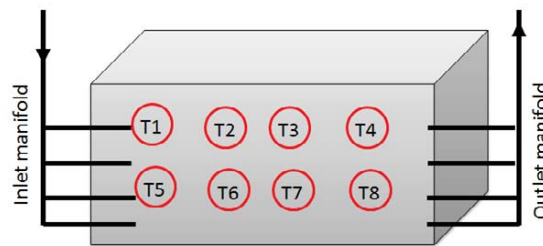

Figure 3: Schematic of the thermocouples position inside the compact heat storage.

3. Experimental testing

3.1. The testing rig

The tests of the prototype have been carried in a testing rig in the laboratory of CNR-ITAE, specifically designed for the characterization of latent heat thermal storages. The layout of the rig is shown in Figure 4, while Figure 5 shows a detail of the hydraulic circuit of the testing bench and the storage connected to it.
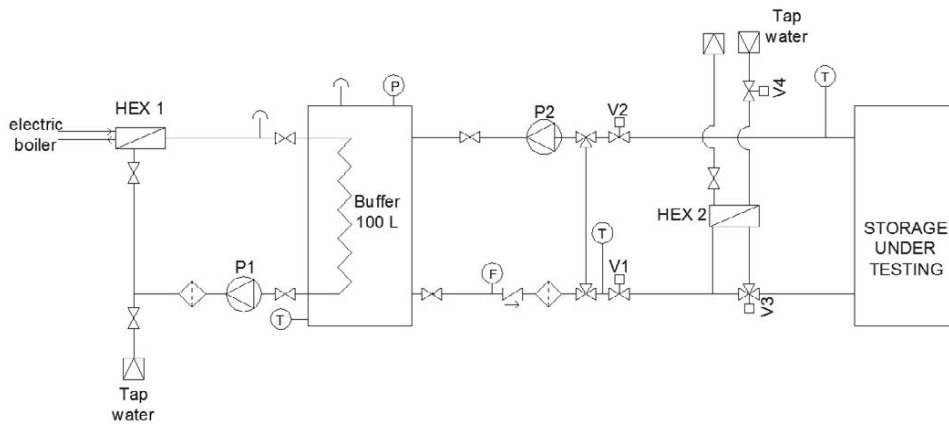
Figure 4: Layout of the test rig for latent heat storage.

Figure 5: detail of the storage during tests.

The main heat source of the testing bench is a 24 kW electric boiler that has been connected to a service buffer, with the aim of providing a constant temperature inlet. A plate heat exchanger is connected, through a mixing valve, to tap water and to the service buffer, thus allowing setting any desired temperature in the range 20°C-85°C for discharge. The management of the testing bench and the acquisition of all the main parameters are made through a software specifically compiled in LabVIEW® environment. For the measure of temperatures, class A thermocouples are used, while a magnetic flow meter with ±1% FS is used for the determination of mass flow rate of the heat transfer fluid (i.e. water). Uncertainty analysis has been carried out for the performed tests, the output showing that uncertainties of 5-8% for all the measured quantities are achieved.

3.2. Methodology

Following Figure 6 schematically represents the steps followed to perform both charging and discharging phase.
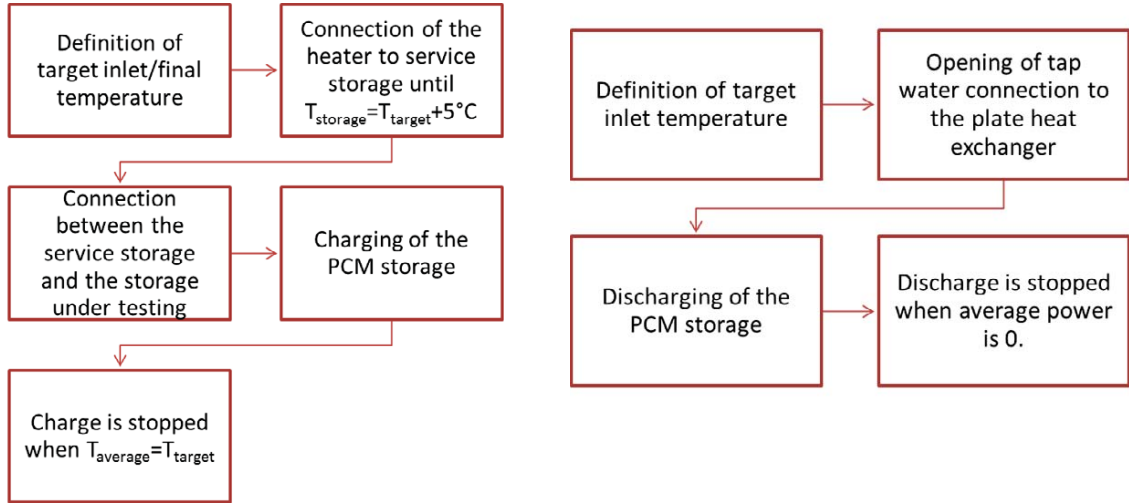
Figure 6: methodology followed for charge and discharge of the storage.

3.3. Calculated figures

The following figures have been calculated for characterization and comparison purposes:

-        Charge/discharge energy, calculated as the integral of the instantaneous power for the whole duration of the charge/discharge process.

$$E = \int_0^{\tau_{fin}} \dot{m} c_p (T_{in} - T_{out}) \cdot d\tau \qquad \text{(eq.1)}$$

-        Average power, calculated as the average of the instantaneous powers for the whole duration of the process.

$$P_{ave} = \frac{\sum_{i=0}^{t_{fin}} \dot{m}_i c_p (T_{in,i} - T_{out,i})}{t_{fin}} \qquad \text{(eq. 2)}$$

-        Charge efficiency, calculated as the theoretical energy given to the system for the phase change over the total one.

$$\varepsilon_{ch} = \frac{E_{th,ch}}{E} \qquad \text{(eq. 3)}$$

-        Discharge efficiency, calculated as the total amount of energy recovered from the system over the theoretical one.

$$\varepsilon_{disch} = \frac{E}{E_{th,disch}} \qquad \text{(eq. 4)}$$

4.   Experimental results

4.1. Charging phase

Figure 7 shows the temperature evolutions of different thermocouples for various tests, differing for the applied flow rate. The same behaviour is shown by all of the sensor: there is an initial rapid increase up to about 75°C, representing the onset temperature of melting, followed by a slower increase, with an almost constant rate until the target temperature is reached and the test is stopped. The curves for T2 and T6 that are placed at two different heights (corresponding to 2 different ranks) show no significant temperature gradients along the height of the system. Instead, marked differences are visible by comparing, for example, the trend for T2 and T4, the

former one in the central part of the heat exchanger while the latter one is near the side wall. Along all the duration of the test a temperature difference of almost 15°C exists between them, mainly due to the poor heat transfer inside the material, which has a low thermal conductivity. It is clear that the material in the central part of the exchanger, which is closer to the fins and especially the tubes, exhibits the highest melting rate, whereas the material on the side of the exchanger even after 5 hours has not completed the phase change. It is interesting to notice that, as already reported in (Cho and Choi, 2000; Torregrosa-Jaime et al., 2013), the melting range is not easily identifiable, since the phase change occurs in a wide range of temperatures. The effect of flow rate is also recognisable: higher flow rates correspond to faster melting dynamics.
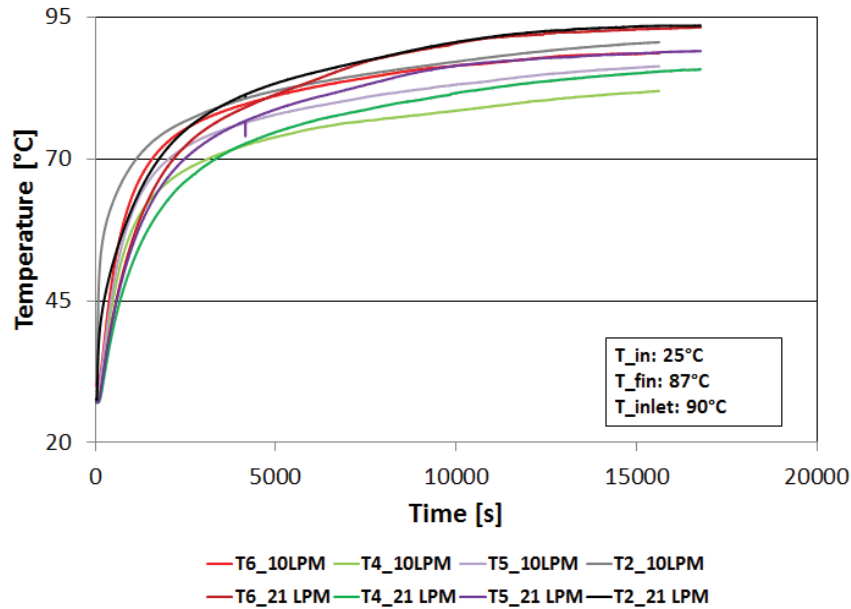

Figure 7: Temperature evolutions of four thermocouples for charging tests at different flow rates.

In Figure 8, efficiency of the storage for charging phase, defined according to eq. 3, is plotted against the temperature difference between the initial and final average temperatures in the storage. Temperature differences from 32°C to 63°C are considered, for two cases, differing in the final temperature reached. From the picture, it is clear that efficiency increases with the temperature difference inside the material, even though in a non-linear manner. The gap in the efficiency for the two series of test, in each condition, lies in the range of 2-4% and therefore is negligible in most conditions. Such a behaviour could be explained considering that, for higher temperature differences, the energy stored includes both the latent heat and a relevant amount of sensible heat, whereas, for lower temperature differences, the highest share in the energy stored is that of latent heat. Indeed, considering that the phase change is a slower process than the sensible heating up, the effect of thermal losses is more relevant when the temperature interval is smaller.
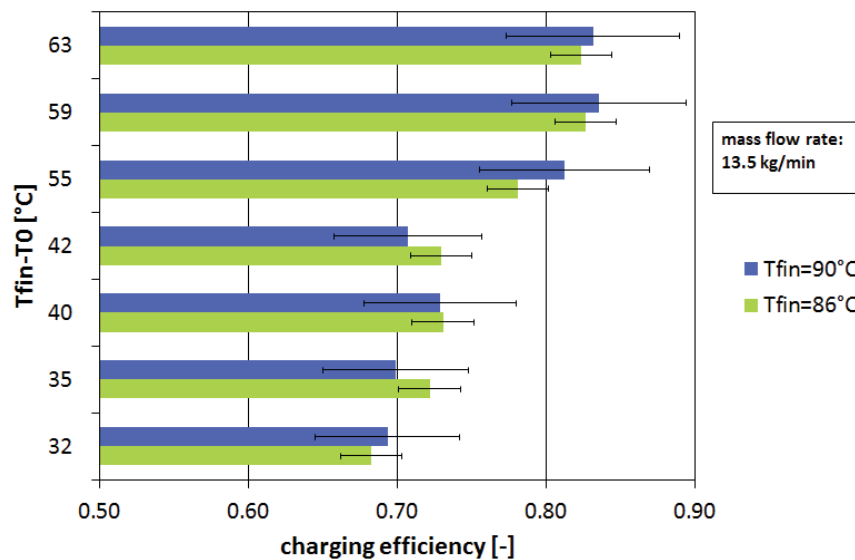
Figure 8: Efficiency vs temperature difference at the beginning and ending of charging tests.

Finally, Figure 9 shows the effect of the mass flow rate of the heat transfer fluid on both the efficiency and the average power supplied. As expected, increasing the average flow rate increases the power input to the storage. At the same time, this has a beneficial effect on the efficiency of the system: since the fluid is in laminar regime, increasing the average flow rate allows enhancing heat transfer from the heat transfer fluid to the material.

4.2. Discharging phase

The melting range of the chosen paraffin is suitable for the collection and storage of low-grade waste heat or solar energy, that are typical heat sources of thermally driven chillers. Considering the typical temperatures for the driving circuit of such chillers, discharging tests with temperatures of 65°C and 70°C were considered.

In Figure 10, the temperature evolutions of two thermocouples at variable flow rates are shown. In particular, the presented sensors are placed in the central part (T3) and in the side of the exchanger (T2). As for the charging phase, a typical behaviour can be identified for T3: at first, the temperature decreases rapidly, until a value of about 85°C is reached. At this temperature, as shown from DSC experiments, solidification starts, and is highlighted in the picture by a decrease of the temperature with a constant slope. Instead, the thermocouple indicated as T4, at the beginning of the examined tests, is around the onset value for solidification and therefore it undergoes a slow constant reduction in temperature for the whole duration of the test. Flow rate has a clear effect on the discharging process of the system, since higher flow rates lead to higher heat transfer dynamics, and therefore a more rapid completion of the phase change process.

In Figure 11, the efficiency of the storage is presented as a function of the initial temperature of the storage. The melting range is highlighted as well, in order to better clarify the results obtained. Indeed, a peculiar trend has been observed: when the initial temperatures are in the range 81°C to 86°C, the efficiency decreases with an increasing of initial temperature, while the efficiency tends to increase when the initial temperature falls below 81°C and when the initial temperature is above than 86°C. This indicates that the efficiency is lower when only the latent heat is released during the tests and increases when part of the sensible heat can be recovered.
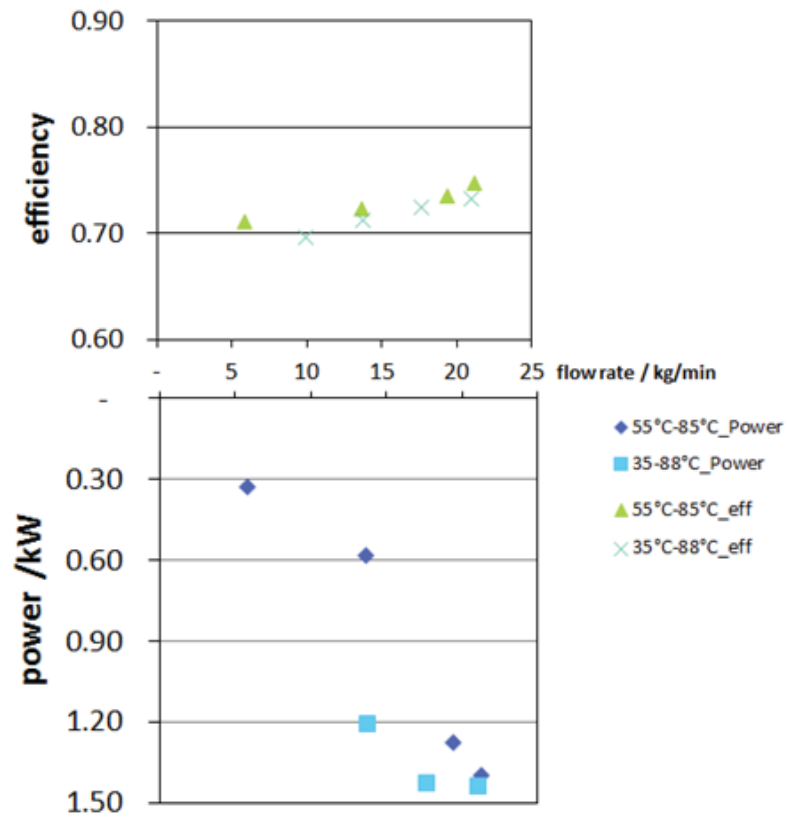
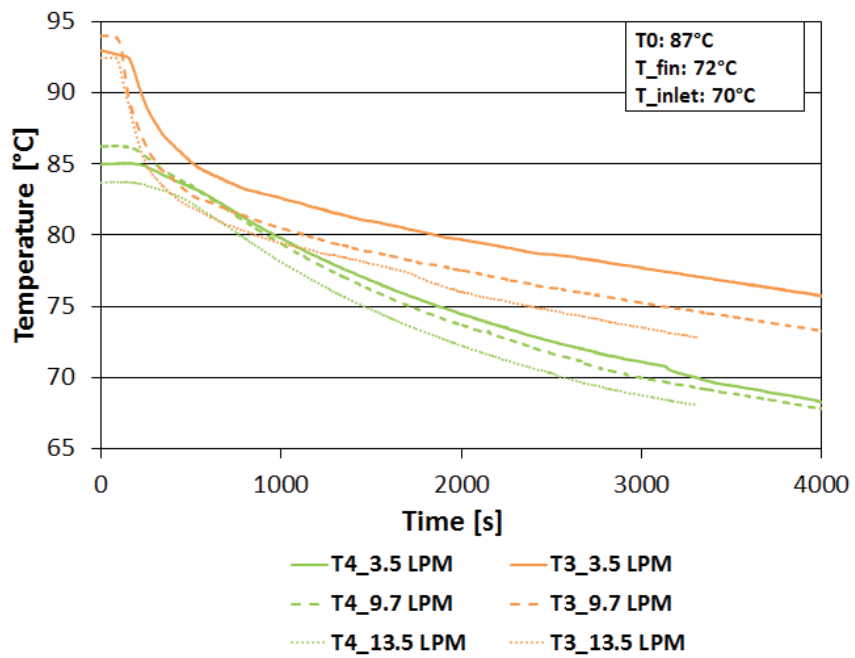**Figure 9: Effect of the flow rate of the heat transfer fluid on the charge of the storage.**

Figure 10: Temperature evolutions inside the storage for three discharging tests at different flow rates.
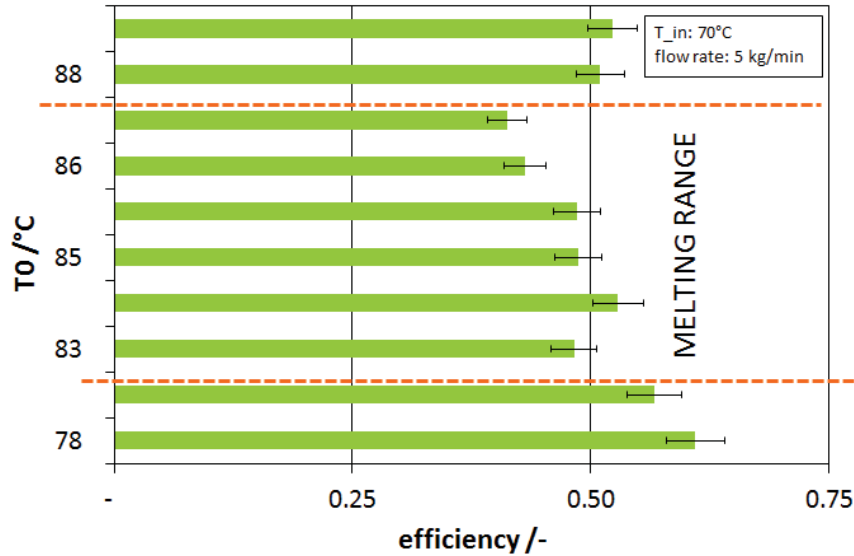
Figure 11: efficiency of the storage for different initial temperature of the storage.

Finally, average discharging power is shown in Figure 12 as a function of flow rate of the heat transfer fluid and average inlet temperature for discharging. The results obtained can be explained by considering that, for the phase change process, the main driving forces are the temperature difference between the storage and the heat transfer fluid, and its flow rate, which affects the rate at which heat is transferred from the fluid to the material on the external side of the pipes. Consequently, the tests with higher temperature of the storage and the lower inlet temperature of the heat transfer fluid correspond to higher power, up to 1.20 kW. The lowest measured powers, for discharging temperature interval of 85°C-70°C and flow rates of 3.5 kg/min or 5 kg/min are of 0.7 kW.
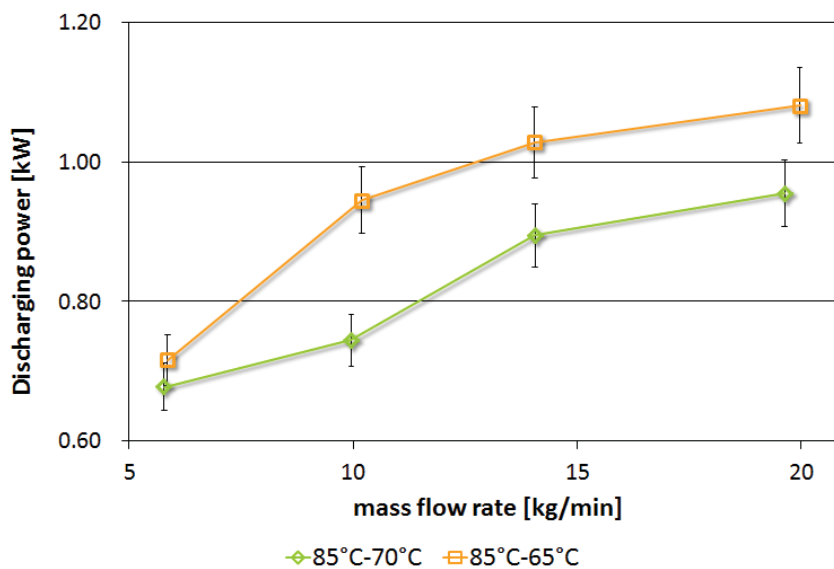

Figure 12: Average discharging power under different boundary conditions.

5. Conclusions

In the present paper, the experimental characterization of a lab-scale latent heat storage for solar cooling application is presented. It is based on the fin-and-tube configuration, employing an organic commercial PCM, PlusIce A82. The experimental outcomes confirmed that the system is characterized by good performance, both in terms of charging/discharging efficiency as well as achievable heat storage density. Indeed, efficiencies ranging between 0.7 and 0.9 during charging and between 0.45 and 0.6 during discharging have been measured.

Furthermore, the energy discharged under typical working conditions corresponds to an energy storage density of about 135 MJ/m^3, which is about 30% higher than a typical sensible heat storage working under the same conditions.

On the contrary, looking at the dynamic performance, in terms of charging and discharging power, it is evident that still the heat transfer efficiency of the system is not optimized. This is due to the intrinsic low thermal conductivity of the PCM as well as to the improper manufacturing of the heat exchangers. Indeed, the fins were not perfectly welded to the tubes, thus adding a high heat transfer resistance, which strongly limits the achievable dynamic performance.

Further investigations are still ongoing to simulate other working boundary conditions typical of a solar cooling plant.

6. Acknowledgements

7. References

Cho, K., Choi, S.H., 2000. Thermal characteristics of paraffin in a spherical capsule during freezing and melting processes, Int. J. Heat Mass Tran. 43, 3183-3196.

Hang, Y., Du, L., Qu, M., Peeta, S., 2013. Multi-objective optimization of integrated solar absorption cooling and heating systems for medium-sized office buildings, Renew. Energ. 52, 67-78.

Henning, H-M., 2007. Solar assisted air conditioning of buildings – an overview. Appl. Therm. Eng. 27, 1734-1749.

Henning, H-M., Motta, M., Mugnier D., 2013. Solar cooling handbook – A guide to solar assisted cooling and dehumidification processes, 3rd Revised & enlarged edition.

Iranmanesh, A., Mehrabian, M.A., 2014. Optimization of a lithium bromide–water solar absorption cooling system with evacuated tube collectors using the genetic algorithm, Energ. Buildings. 85, 427-435.

Mehling, H., Cabeza, L.F., 2008. Heat and cold storage with PCM, Ed. Springer.

Monné, C., Alonso, S., Palacín, F., Serra, L., 2011. Monitoring and simulation of an existing solar powered absorption cooling system in Zaragoza (Spain). Appl. Therm. Eng. 31, 28-35.

Talmatsky, E., Kribus, A., 2008. PCM storage for solar DHW: An unfulfilled promise?, Sol. Energy. 82, 861-869.

Torregrosa-Jaime, B., Lopez-Navarro, A., Corberan, J.M., Esteban-Matias, J.C., Klinkner, L., Payà, J., 2013. Experimental analysis of a paraffin-based cold storage tank, Int. J. Ref. 36, 1632-1640

World Business Council for Sustainable Development (WBCSD), Energy Efficiency in Buildings Facts and Trends, Full Report, 2008.

NOMENCLATURE

Quantity	Symbol	Unit
Energy	E	J
Mass flow rate	$\dot{m}$	kg/min
Power	P	kW
Specific heat	c_p	J kg^{-1} K^{-1}
Temperature	T	K
Time steps	t	-
Efficiency	ε	
Time	τ	s
Subscripts		
charging	ch	
discharging	disch	
final	fin	
initial	0	

inlet	in
outlet	out
theoretical	th